Journal of Materials Chemistry B

Accepted Manuscript

ROYAL SOCIETY OF CHEMISTRY

www.rsc.org/materialsB

In Vitro and *In Vivo* Drug Release Behavior and Osteogenic Potential of A Composite Scaffold Based on Poly(*ε*-caprolactone)-*block*-poly(lactic-*co*-glycolic acid) and *β*-tricalcium Phosphate

Pei Zhao,[a,b,l] Dawei Li,[c,l] Fei Yang,[b,*] Yuanzheng Ma,[c] Tiantian Wang,[c] Shun Duan,[a] Hong Shen,[b] Qing Cai,[a,*] Decheng Wu,[b] Xiaoping Yang[a] and Shenguo Wang[b]

Abstract

To cure serious bone tuberculosis, a novel long-term drug delivery system was designed and prepared to satisfy the needs of both bone regeneration and antituberculous drug therapy. The antituberculous drug (rifampicin, RFP) was loaded into a porous scaffold, which composed of a new designed polylactone, poly(*ε*-caprolactone)-*block*-poly(lactic-*co*-glycolic acid) (*b*-PLGC) copolymer, and *β*-tricalcium phosphate (*β*-TCP). The releasing results demonstrated that RFP could be steadily released for as long as 12 weeks both *in vitro* and *in vivo*. Within the *in vivo* experimental period, the drug concentration in tissues surrounding implants was much higher than that of in blood which was still superior to the effective value to kill mycobacterium tuberculosis. MC3T3-E1 osteoblasts proliferated well in extracts and co-culture on composite scaffolds, indicating good cytocompatibility and cell affinity of the scaffold. The results of rabbit radius repair experiment displayed the scaffold has good bone regeneration capacity. The RFP-loaded *b*-PLGC/TCP composite

scaffold thus could be envisioned to be a potential and promising substrate in clinical treatment of bone tuberculosis.

Keywords: bone tuberculosis therapy, composite scaffold, drug delivery, bone regeneration.

1. Introduction

Tuberculosis (TB), caused by the mycobacterium tuberculosis, continues to present a formidable challenge to humans. According to the World Health Organization's 2014 global report, there were an estimated 9.0 million new cases of TB and 1.5 million people died from TB in 2013.[1,2] Classified by the infection parts of body, there are two kinds of TB, pulmonary and extra-pulmonary. Bone TB is the most significant extra-pulmonary TB for its large number of infection cases and serious consequences. There are about 19-38 million bone TB cases around the world, most of which are the secondary disease of pulmonary TB.[3-6] Many funds and efforts had been spent on pulmonary TB, while little attention was paid to bone TB.

The most common method in treating serious bone TB cases is the infection foci debridement with a subsequent internal fixation.[7] However, the tuberculosis bacillus is hard to be cleaned up completely after debridement operation. Some of them will survive and become latent bacillus which would reproduce rapidly once in suitable conditions.[8] Hence, apart from the debridement operation, antitubercular drug therapy is still necessary for a long period. A general strategy for these patients is chemotherapy by oral administration or intravenous injection for 9 to 12 months, which is undoubtedly a heavy burden to patients.[9,10] In addition, to achieve effective local drug concentrations, patients have to take excess drug on a long-term to obtain

high blood drug concentration, which might cause serious toxic effect to tissues and organs, especially liver and kidney.[11] Besides, bioavailability of anti-mycobacterial drugs is another major clinical problem. Rifampicin (RFP), one of the first-line antitubercular drugs, shows a decline in intestinal absorption, and tends to undergo fast and great decomposition in stomach in case of other antitubercular drugs presenting.[12-14] Local drug delivery system (DDS) offers an effective approach for the drug therapy of bone TB. It possesses advantages of specific site delivery, drug dosage optimizer and release duration. Moreover, patient compliances will be no longer a hard-to-predict trouble affected curative effect.[15-17]

On the other hand, the debridement of infected bone by TB leaves a residual cavity, which is liable to cause a rising opportunity of common bacterial infection and rapid propagation of the residual tuberculosis bacterial. Hence, the cavity should be filled to avoid the infection and help the regeneration of new tissue.[8] Apart from autologous and allogeneic bone transplantation, bone regeneration basing on the concept of bone tissue engineering has been identified to be an effective way to remodel the bone defects and restore the function.[18-20] Due to their biocompatibility and flexibility in biodegradation rates, aliphatic polylactones are the most widely used polymeric biomaterials.[21-24] Inorganic compounds such as calcium phosphate are usually incorporated into polylactone scaffolds to enhance osteogenesis.[25-27] In numerous published data, bone repair have been reported using polylactone/calcium phosphate organic-inorganic composite scaffolds.[28-30]

With all these considerations, antitubercular drug-loading polylactone/calcium phosphate organic-inorganic composite scaffolds would be a promising solution to satisfy the needs of both bone regeneration and antituberculous drug therapy in treating bone TB. Actually, polylactone scaffolds have been widely served as carriers

for growth factors, anti-inflammatory and anti-cancer drugs. For example, Jung and coworkers designed BMP-7 loaded poly(lactide-*co*-glycolide) (PLGA) scaffold that could retain the dual-function of local BMP-7 release and progenitor-scaffolding with its defect-fitting architecture.[31] Petit and coworkers reported a celecoxib-loaded scaffold based on acetyl-capped PCLA-PEG-PCLA triblock copolymer.[32]

Herein, RFP-loading organic-inorganic composite scaffolds were designed and prepared using a polylactone and *β*-tricalcium phosphate (*β*-TCP). The main strategies of drug loading include chemical bonding and physical bleeding. Kang and coworkers designed kartogenin-conjugated chitosan nano/microparticles for cartilage regeneration.[33] Feng and coworkers designed a conjugated polymer nanoparticle by electrostatic assembly of cationic conjugated polymer PFO and anionic poly(L-glutamic acid) conjugated with anticancer drug doxorubicin (PFO/PG-Dox).[34] A previous work of our laboratory by Huang and coworkers designed an isoniazid conjugated star poly(lactide-*co*-glycolide) and blend with *β*-TCP to fabricate bone tissue-engineered scaffolds, which realized a rather long time of drug release.[35] However, the main obstacles in such designs included possible drug degeneration and incomplete drug release, in particular the possible change of pharmacological effect after the chemical bonding and during the degradation of the polymer. When its molecular weight is lower than 5000, the degraded fragment of polylactone linked with drug molecule can be dissolved in water and it is considered as a drug molecule, but whether it can play the role as the same of a drug molecule is doubtful. Physical blending does not change the chemical properties of the drug, from this the safety and effectiveness are guaranteed. Hence, we choose physical blending to form the drug delivery system. But still there are some problems unsolved in the drug release behavior in the reported researches by now including initial burst release, uneven

release behavior and short drug release duration less than 40 days.

The main points of this study include improvement of the uniformity and extension of the release duration, and suppression of the initial burst release as possible. The release behavior is mainly controlled by the degradation and drug permeability of the polymer but not just the former. Therefore, we design a polylactone to adjust both of the degradation and drug permeability properties as far as possible to overcome the shortcomings. Since PCL has high permeability for drug molecules, while PLGA has flexibility in degradation adjustment, *b*-PLGC was synthesized with the purpose of getting both desired RFP releasing behavior and degradation rate. RFP release behaviors *in vitro* and *in vivo* reflected RFP concentrations obtained in blood and tissue surrounding the implant could reach a high value, which was above the effective level required for TB treatment. The RFP/*b*-PLGC/TCP scaffold showed good cytocompatibility in *in vitro* assessment by MC3T3-E1 cell culture and good bone regeneration capacity, as well as the *b*-PLGC/TCP scaffold in the animal tests. In a word, the RFP/*b*-PLGC/TCP scaffold should have the great potential to combine recovering the residual cavity and the drug therapy for effective bone TB treatment.

2. Experimental section

2.1 Materials

L-lactide and glycolide were purchased from PURAC (the Netherlands) and purified by recrystallization in anhydrous ethyl acetate twice. Ethyl acetate was dried by P_2O_5 overnight and then distilled. *ε*-Caprolactone was purchased from Acros Chemica (Belgium), dried with calcium hydride for 24 h, and distilled under vacuum (82 ^{o}C/133 Pa). Stannous octoate (Sigma, A.R.) was used directly without further purification.

NaCl of analytical quality was purchased from Beijing Chemical Works, China. It was sieved and particles with diameter 150-250 μm were selected. *β*-TCP powders with diameter 300-500 nm were purchased from the Forth Reagent Factory of Shanghai, China. RFP was purchased from Energy Chemical, China. 1,4-Dioxane, chloroform and other reagents were of analytical grade and used without further purification.

2.2 Preparation and characterization of polylactones

b-PLGC copolymer was synthesized via two steps according to our previous report.[36] As shown in Scheme 1, firstly, mixture of *ε*-caprolactone (CL) and hexadecanol were put into a polymerization tube, and then 0.05 wt% stannous octoate was added as catalyst. After deoxygenating with pure argon, the tube was sealed under vacuum and then immersed in an oil bath thermoset at 140 ^{o}C for 20 h. Purified PCL pre-polymer was obtained by dissolving the product in chloroform, followed by precipitation from ethanol. Subsequently, PCL pre-polymer, glycolide and lactide, as well as 0.05 wt% stannous octoate, were sealed into a glass tube under vacuum after deoxygenating with pure argon. The tube was immersed in oil bath and kept at 160 ^{o}C for 20 h. The raw product was purified by precipitating its solution in chloroform into ethanol, and then dried thoroughly under vacuum at room temperature. Poly(L-lactide-*co*-glycolide) (PLGA), poly(L-lactide-*co*-glycolide-*co*-caprolactone) (*r*-PLGC) and poly(L-lactide) (PLLA) were synthesized and purified under same condition to that of *b*-PLGC (160 ^{o}C, 20 h).

^{1}H NMR spectra were obtained with ADVANCE 400 spectrometer (Bruker, German) at room temperature, using $CDCl_3$ as solvent and tetramethylsilane (TMS) as internal reference. GPC measurements were carried out on GPCmax VE-2001 (Viscotek, UK) maintained at 35 ^{o}C. Tetrahydrofuran or chloroform was used as the

eluent at a flow rate of 1.0 mL·min^{-1}; calibration was performed with polystyrene standards. Polylactone films were fabricated by solution-casting and water contact angles were measured using a Contact Angle Meter (JC2000C1, Zhongchen, China). Ten independent determinations at different sites of a film were averaged. Differential scanning calorimetry (DSC) measurements were carried out on a differential scanning calorimeter (Q2000, Ta instruments, American) at a heating rate of 10 ^{o}C·min^{-1}. Thermograms covering a range of -60 ^{o}C to 200 ^{o}C were recorded and the glass transition temperature (T_g) and melting point (T_m) of different polylactones were identified according to the thermograms.

2.3 Preparation and characterization of RFP-loaded polylactone/TCP composite scaffolds

To ensure interpenetrated porous structure, scaffolds were fabricated by a particle leaching in combination with phase separation technique referring to our previous study.[37] Briefly, mixtures of polylactone, TCP and RFP (1.0/1.0/0.2 in w/w/w) were put into 1,4-dioxane to form slurry of 10 wt% polylactone solution. Pre-sieved NaCl particles (150-300 μm in diameter) were then added into the slurry at a weight ratio of 20/1 to the total weight of polylactone and TCP. The paste was then fit into a mold, frozen under -20 ^{o}C, and freeze-dried for 48 h. RFP-loaded polylactone/TCP scaffolds were obtained after NaCl particles were washed away completely with distilled water and freeze-dried for 24 h. RFP-free polylactone/TCP scaffolds were fabricated in a similar way except on RFP being introduced into the slurry. All scaffolds were cut into cylindrical pieces with the size of approximately 5 mm in diameter and 10 mm in thickness with about 300 mg, and then stored at 4 ^{o}C for further use.

Morphologies of polylactone/TCP scaffolds were characterized using scanning electron microscope (SEM, JSM-6700F, JEOL Ltd, Japan) after the scaffolds was

coated with gold using a sputter coater (E-1010, Hitachi Ltd, Japan). Pore sizes were measured using ImageJ software (National Institutes of Health, USA) according to the SEM micrographs. For each scaffold, the averaged diameter of the pores was calculated basing on 100 measurements. The porosity of the scaffolds was determined as described previously.[38] The loading efficiencies of RFP in polylactone/TCP scaffolds were measured as follows: Twenty milligrams of RFP-loaded scaffolds were dissolved in 10 mL dichloromethane and the solution was centrifuged at 8000 rpm for 10 min to remove TCP particles. The clear solution was analyzed using UV spectrophotometer (TU-1901, PERSEE, China) at λ_{max} = 474 nm. And the same quality of pure scaffolds was treated with the same way to the RFP-loaded scaffolds and the clear solutions were used as control. The concentration of RFP was calculated with a calibration curve from RFP standard solutions at different concentrations. The percent drug loading and percent encapsulation efficiency were calculated as follows:

$$\text{RFP loading content}\,(\%) = \frac{\text{weight of RFP in scaffold}}{\text{weight of RFP} - \text{loaded scaffold}} \times 100\%$$

$$\text{RFP entrapment efficiency}(\%) = \frac{\text{weight of RFP in scaffold}}{\text{weight of RFP feeding}} \times 100\%$$

2.4 *In vitro* release behaviors of RFP from composite scaffolds

Release behaviors of RFP-loaded polylactone/TCP composite scaffolds *in vitro* were carried out at 37 ^{o}C in 10 mL of 0.1 M PBS (pH = 7.4). The release medium was withdrawn at pre-determined time intervals, and replaced with a fresh soaking medium each time. Then the concentrations of RFP were determined by UV spectrophotometer by measuring the maximum absorbance at the 474 nm, respectively. The concentration of RFP was calculated with a calibration curve from RFP standard solutions at different concentrations.

2.5 *In vitro* cytotoxicity evaluation

Polylactone/TCP scaffolds were soaked in DMEM (Hyclone) for 24 h, and the extracts were used for cell culture. MC3T3-E1 (5×10^3 cells/well) was seeded into 96-well plates, and incubated with extracts at 37 ^oC in humidified atmosphere with 5% CO_2, using DMEM as control. Cell proliferation rates were tested by CCK-8 method. Briefly, at day 1, 3, 5, and 7 after seeding, 20 μL of CCK-8 solution was added into each well and incubated at 37 ^oC for 4 h, and then the OD value was measured by microreader (Model 680, Bio - rad, American) at the wavelength of 490 nm. Cell number was calculated by a standard curve. MC3T3-E1 (1×10^4 cells/well) was seeded onto composite scaffolds (5 mm in diameter and 1 mm in thickness) in 48-well plates and cultured with DMEM supplemented with 10% fetal bovine serum (FBS, PAA, Germany), 100 IU·mL^{-1} penicillin (Sigma), and 100 mg·mL^{-1} streptomycin (Sigma). Tissue culture polystyrene (TCPS) was taken as control. SEM micrographs were taken when cells had attached and proliferated on scaffolds for 3 days. The samples were fixed in 2.5% glutaraldehyde and serially dehydrated with an increasing ethanol gradient, air-dried in a hood and sputter-coated with gold prior to imaging under SEM at 5 kV.

2.6 *In vivo* osteogenesis evaluation

Animals and surgical procedures. The study was conducted under a protocol approved by the institutional animal care and uses committee of the 309th Hospital of PLA and performed in accordance with the Guide for Care and Use of Laboratory Animals. Twenty-seven skeletally mature New Zealand rabbits (about 3 kg of weight) were used. Rabbits were divided randomly into three groups: (1) 9 defects for implantation of *b*-PLGC/TCP scaffold; (2) 9 defects for implantation of RFP/*b*-PLGC/TCP scaffold; (3) 9 defects were left untreated as blank control.

Surgery was carried out under sterile condition to establish a model with

critical-sized segmental defect, started with intramuscular anesthesia of rabbits by 3% pentobarbital sodium (30 mg·kg^{-1}). After shaving off hair on the right forelimb, a longitudinal skin and musculature incision measuring approximately 20 mm was made at the anteromedial aspect. A unilateral segment of the periosteum and radius with 10 mm in length and 5 mm in diameter was removed in the middle of radius by using a hard drill. The defect was subsequently irrigated with physiological saline and filled with scaffold aforementioned and the size of scaffolds was consistent with that of the defect. Finally, the underlying musculature and skin were sutured, and the wound was covered by sterile gauze. Infection was prevented with a single intramuscular injection of gentamicin (10,000 IU·kg^{-1}) immediately after surgery. Rabbits from each group were sacrificed by lethal intravenous administration of sodium pentobarbital at 4, 8, 12 weeks post-implantation, respectively.

***In vivo* drug concentration in blood and tissue.** At 4, 8, and 12 weeks post-surgery, 1 mL blood samples were immediately collected from ear veins after the rabbits were sacrificed. In addition, the blood samples were also collected from five randomly selected normal rabbits. The blood specimens were all centrifuged and the blood serums were obtained. And the blood serums were precipitated into methanol and centrifuged, and then the supernatants were collected. And samples of bones (0.5 cm away from the closer end of the groove), musculature and fibrous tissue cling to the groove and tissues were collected as well. The tissues were weighted and added into 2 mL saline before being homogenate. 1.0 mL of the tissue suspension was mixed with 2.0 mL methanol. The homogeneous mixture was centrifuged and the supernatants were reserved. The concentration of drug distributed in blood and tissues were investigated by UV spectrophotometer by measuring the maximum absorbance at 474 nm.

Radiological examination. Rabbits from each group anesthetized by injecting ketamine (10 $mg \cdot kg^{-1}$) and Sumianxin II (0.1 $mL \cdot kg^{-1}$) via ear vein at 4, 8 and 12 weeks after implantation, respectively. Then, the rabbits were radiographically examined by X-ray microradiography (Philips class-type B). An appropriate magnification was applied throughout the observation. The degree of new bone formation during the healing period was estimated using the grey scale.

Histological analysis. The tissue samples were fixed in 10% neutral buffered formalin for 7 days, decalcified and dehydrated according to standard protocols, embedded in paraffin and sectioned at 5 μm thickness. H&E staining and Masson's trichrome staining were performed separately on tissue sections, according to the manufacturer's protocols, and images were captured under light microscope (CX21, Olympus, Japan).

Immunohistochemical analysis. Immunohistochemistry for osteocalcin (OC) was performed according to the literature.[39] Briefly, tissue sections were de-paraffinised and rehydrated then submerged in hydrogen peroxide to quench peroxidase activity. Before exposure to the primary antibody against OCG3 (ab13420, Abcam, dilution 1/500), Tissue sections were incubated with 1% BSA to block nonspecific binding. After incubation with primary antibody overnight at 4 ^{o}C, HRP conjugated secondary antibody was applied to the tissue sections for 1 h at room temperature. Finally, the dia-minobenzidine (DAB, Beyotime, Jiangsu, China) kit was used to develop the color, followed by counterstaining with hematoxylin. Tissue sections were observed under a light microscope (CX21, Olympus, Japan). OC expression within the defect area was quantified using a web application software ImunoRatio.

2.7 Statistical analysis

All quantitative data were expressed as mean ± standard deviation (n = 3).

Statistical analysis was made based on t-test, and differences between groups were considered as significant for $p < 0.05$.

3. Results and discussion

3.1 Synthesis and characterization of polylactones

Polylactones, including PLLA, PLGA, PCL, and PEG block derivatives, approved by FDA for biomedical use, are the most popular biodegradable and biocompatible polymers for drug delivery and tissue engineering.[40,41] In this study, a novel block polylactone, poly (ε-caprolactone)-*block*-poly (lactic-*co*-glycolic acid) (*b*-PLGC) copolymer, was synthesized by two steps of ring-opening polymerization, as shown in Scheme 1. Firstly, PCL pre-polymer with expected molecular weight was synthesized by the ring-opening polymerization of ε-caprolactone with hexadecanol as initiator. And then PCL prepolymer, glycolide and lactide (feeding mole ratio of LA/GA/CL was 63/27/10) were adopted to synthesize *b*-PLGC copolymer. Besides, to compare the influence of micro-segment structure on drug release behavior, *r*-PLGC (63/27/10) copolymer was synthesized by direct polymerization of LA, GA and CL. Commonly used PLGA (70/30) and PLLA were also synthesized by the similar method for comparison. In order to eliminate the effect of deviations in molar ratios and molecular weights of different polylactones on drug release behaviors, the molar ratios of LA/GA in both PLGC and PLGA were theoretically controlled at 70/30, and the molecular weights of all the polylactone were adjusted in similar values. As shown in Table 1, the weight-average molecular weights (M_w) measured by GPC were all in the range of 80 kDa-100 kDa, and the practical chemical compositions determined by ^{1}H NMR was close to the feeding doses.

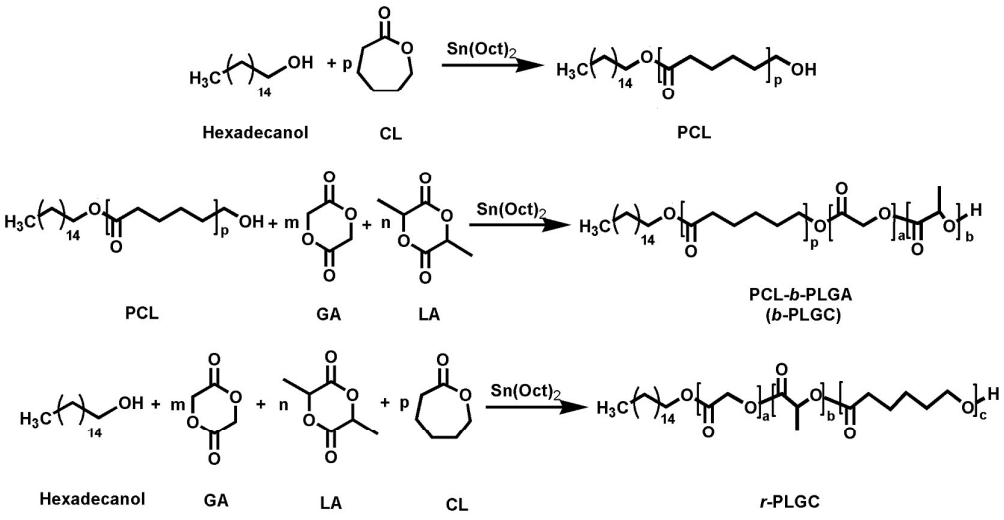

Scheme 1 Synthesis of *b*-PLGC and *r*-PLGC copolymers.

It was well known that the hydrophility/hydrophobicity ratio and crystallization morphology (especially at body temperature 37 ^{o}C) of polylactones had great influence on their degradation rates and drug release behaviors.[42,43] According to the Table 1, PLLA, crystalline polymer, has a clear melting peak at 189 ^{o}C, while the amorphous polymers like PLGA and *r*-PLGC, have no melting peak. Notably, the T_g of *r*-PLGC is much lower than those of the others, which implied it was in rubbery state at 37 ^{o}C. *b*-PLGC showed two T_g at -60 ^{o}C and 67.5 ^{o}C, respectively, which demonstrated that it presented a two-phase structure, i.e. PCL crystalline and PLGA amorphous domains.[36] As we all have known, PCL has been widely used as drug carrier material owing to its excellent drug permeability, but its low degradation rate restrains its application in tissue engineering.[44] Whereas, the copolymerization of PCL with glycolide and lactide could accelerate its degradation rate and keep its good drug permeability, and may have advantage in tissue engineering.

Table 1 The major characteristics of polylactones.

Sample	GPC			Molar ratio[a] (LA/GA/CL)	Contact angle (degree)	T_g (^oC)	T_m (^oC)
	M_n	M_w	PDI				
PLLA	82,000	99,000	1.21	100.0/0.0/0.0	81.0	70.0	189.0
PLGA	69,000	101,000	1.47	68.5/31.5/0.0	67.5	60.3	-
r-PLGC	67,000	84,000	1.25	61.5/27.7/10.8	69.5	26.7	-
PCL	17,000	24,000	1.41	0.0/0.0/100.0	88.6	-60.0	53.1
b-PLGC	64,000	88,000	1.38	62.3/26.5/11.2	70.2	-60.0, 67.0	53.5

[a]Calculated from ^{1}H NMR measurement.

3.2 Preparation and characterization of RFP/polylactone/TCP scaffolds

Commonly, scaffolds used in bone regeneration should be three-dimensional and highly porous with an interconnected network of pores (at least 100 μm) to allow cell migration, tissue in-growth and vascularization.[45,46] In order to fabricate suitable scaffolds, various processing techniques such as electrospinning, self-assembly, salt-particle leaching, 3D-printing et al, have being developed to design and prepare scaffolds. In this study, four different RFP-loaded polylactone/TCP scaffolds, including PLLA, PLGA, *r*-PLGC, *b*-PLGC containing the same amount of TCP, were fabricated by particle leaching using NaCl as porogen in combination with phase separation/freeze drying technique.

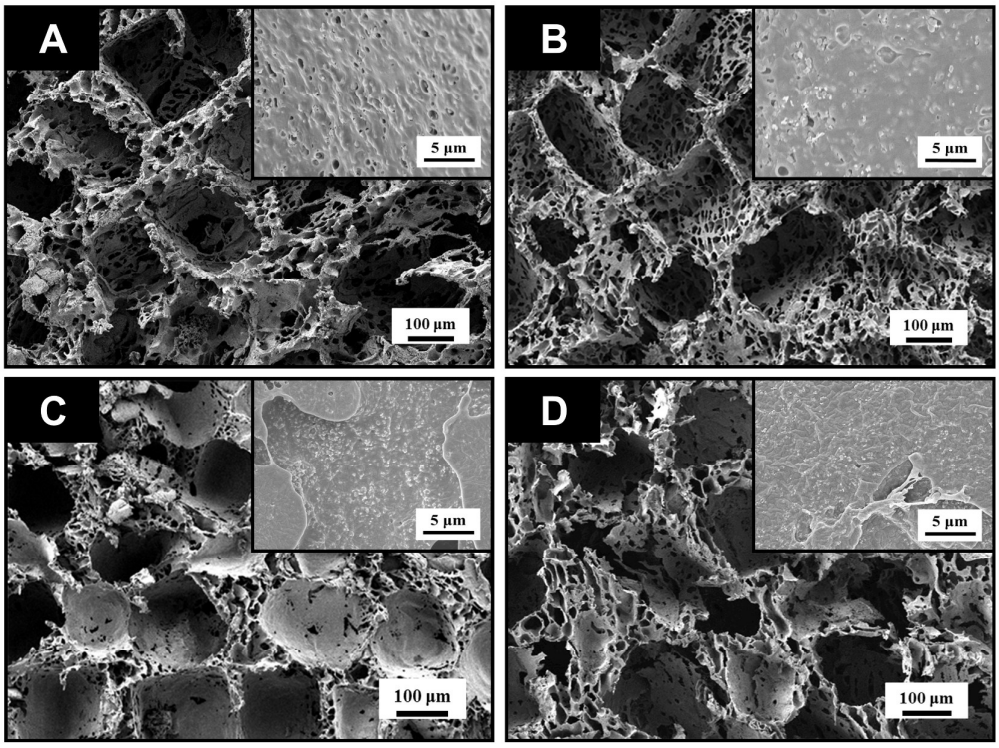

Fig. 2 SEM images of the RFP/polylactone/TCP composite scaffolds. A. RFP/PLLA/TCP scaffold; B. RFP/PLGA/TCP scaffold; C. RFP/*r*-PLGC/TCP scaffold; D. RFP/*b*-PLGC/TCP scaffold.

Morphological characterizations of these scaffolds were determined by SEM observation as shown in Fig. 2. All the scaffolds possessed similar 3-D random porous structure and TCP distributed uniformly in the polymer matrix. The main pore parameters determined from SEM images and corresponding porosities were shown in Table 2. All the scaffolds exhibited similar porosity about 85%-90%, and the pore sizes of these scaffolds fell in a range of 200-300 μm. Numerous micro-pores (10-50 μm) could be observed on the wall of macro-pores, which provided a high surface area for maximizing cell seeding and attachment, sufficient space for extracellular matrix (ECM) regeneration and minimal diffusion constraints. Porous structure of scaffolds and drug loading could be conducive to the release of RFP from scaffolds. As shown in Table 2, the RFP loadings of all scaffolds were 3.2%-4.6%. Therefore,

the similarity in pore size, porous structure and drug loading for all scaffolds demonstrated that the following RFP release behaviors would be mainly dependent on physiochemical properties of polylactones.

Table 2 Major pore parameters, RFP loading and entrapment efficiency of RFP/polylactone/TCP scaffolds.

Parameters	Scaffolds			
	RFP/PLLA/TCP	RFP/PLGA/TCP	RFP/*r*-PLGC/TCP	RFP/*b*-PLGC/TCP
Average pore diameter (μm)	246.0±43.0	229.0±47.0	210.0±29.0	256.0±46.0
Porosity (%)	89.0±1.3	85.3±1.8	83.4±1.2	86.7±0.8
RFP loading[a] (%)	4.6±0.4	4.4±0.5	3.2±0.7	3.5±0.5
Entrapment efficient (%)	46.0±4.0	44.0±5.0	32.0±7.0	35.0±5.0

[a]Feeding dose of polylactone/TCP scaffold was 10% (wt%).

3.3 RFP release behaviors *in vitro* and *in vivo*

The release profiles of RFP from different polylactone/TCP scaffolds *in vitro* are shown in Fig. 3(A). A slight burst release occurred in all cases at the first day, which accounted for ~35% of the total loaded RFP from the *r*-PLGC/TCP scaffold, while ~20% from the other three scaffolds. After the initial burst release, different release profiles were obtained from different scaffolds. The RFP release from both PLLA/TCP and PLGA/TCP scaffolds became quite slow. For instance, the cumulative release from PLGA/TCP scaffold reached only ~55% at 14 days and ~65% at 84 days. The RFP release from PLLA/TCP scaffold was further slower than that from PLGA/TCP scaffold. On the contrary, the RFP release from *r*-PLGC/TCP scaffold was very fast that almost 90% of total RFP had been released within 63 days. However, a long-term sustained RFP release was obtained for the sample of *b*-PLGC/TCP scaffold. RFP could be seen releasing from *b*-PLGC/TCP scaffold at a kind of approximate linear rate during the whole experimental period, in which, 3.17±0.15% of RFP was released per week.

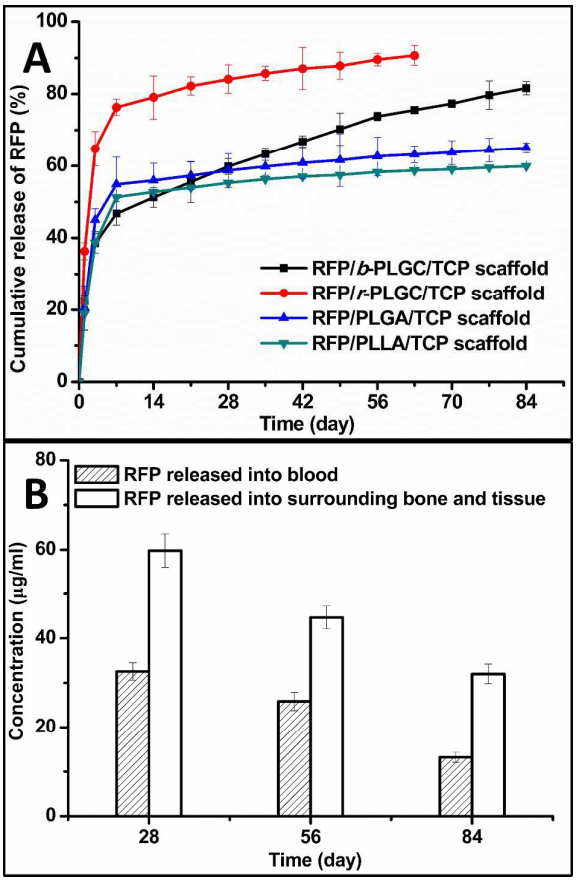

Fig. 3 Release behaviors of RFP from composite scaffolds *in vitro* (A); Concentrations of RFP released from RFP/*b*-PLGC/TCP scaffold into blood or surrounding bone and tissue *in vivo* (B).

The initial burst release from all the scaffolds should be attributed to those RFP molecules existing on surface of the substrate. In preparing the scaffolds, RFP was dissolved in polymeric solution and mixed well with polylactone/TCP slurry. Therefore, there always should be some RFP existing on or close to the scaffold surface, which likely lead to the initial burst release. Those RFP molecules embedded inside polymeric matrixes would be released via steps of water molecules interpenetration and RFP diffusion out, in which, the physiochemical features of polymeric matrix played important roles in regulating release behaviors.[47] RFP is hydrophobic and its solubility in water is limited. It was understandable that the release of hydrophobic RFP from hydrophobic PLLA/TCP and PLGA/TCP scaffolds

in aqueous environment was slow after the initial burst release. However, it has been reported that the diffusion coefficient of lipophilic drug was much larger in PCL than in PLA and PLGA.[36] Thus, addition of the CL component into PLGA should be able to accelerate the rate of RFP release, as indicated by the cases of *b*-PLGC/TCP and *r*-PLGC/TCP scaffolds. In comparison with *b*-PLGC/TCP scaffold, the significantly faster RFP release rate of *r*-PLGC/TCP scaffold result from its rubbery state at 37 ^{o}C. As shown in Table 1, only *r*-PLGC distinctly displayed a T_g below 37 ^{o}C. Movements of chain segments are much easier in rubbery state than in glassy state, which apparently facilitate the water interpenetration in and RFP diffusion out of the *r*-PLGC scaffold. While for *b*-PLGC/TCP scaffold, the presence of PCL block enhanced the diffusion of RFP, accelerated the release rate, therefore, a sustained release behavior was resulted as expected in comparison with other three cases.

Since *b*-PLGC/TCP scaffold could achieve continuous RFP release as long as ~3 months, the RFP/*b*-PLGC/TCP scaffold was chosen and implanted into the rabbit radius defect to test its release behavior *in vivo*. The released RFP would diffuse into surrounding tissues or enter into blood, therefore, blood and tissue samples were collected at 4, 8 and 12 weeks after surgery, and the RFP concentrations in these samples were monitored with UV spectrophotometer (Fig. 3(B)). The mean maximum RFP concentration in blood was 32.55±1.98 μg·mL^{-1} at the fourth week. It decreased with longer implantation time, and it was 13.21±1.10 μg·mL^{-1} at week 12 after implantation, which was still higher than the reported effective therapeutical concentration (5 μg·mL^{-1}).[8] The levels of RFP in surrounding bone tissue were detected much higher than those in blood samples at all-time points. At week 4, for instance, it was 59.79±3.76 μg·mL^{-1} in bone tissue, which was almost two times of that in blood. To the week 12 after implantation, the RFP concentration in tissue

remained as high as 32.01 ± 2.21 μg·mL^{-1} Clearly, the RFP released from *b*-PLGC/TCP scaffold should be effective in treating bone TB.

3.4 Cytocompatibility of RFP/polylactone/TCP scaffold

With the continuous release of anti-TB drug, it was important to evaluate the cytocompatibility of RFP-loaded scaffolds *in vitro* before they were applied to treat bone TB. It was reported that RFP exerted deleterious effects on osteoblast growth and differentiation at concentrations exceeding 50 μg·mL^{-1}, consistent with its inhibitory effects on DNA synthesis.[48,49] Hence, *in vitro* culture of MC3T3-E1 osteoblasts in extracts from RFP/polylactone/TCP scaffolds or directly on the scaffolds was conducted using polylactone/TCP scaffolds as references, and cytotoxicity was evaluated by observations on cell adhesion, ingrowth and proliferation.

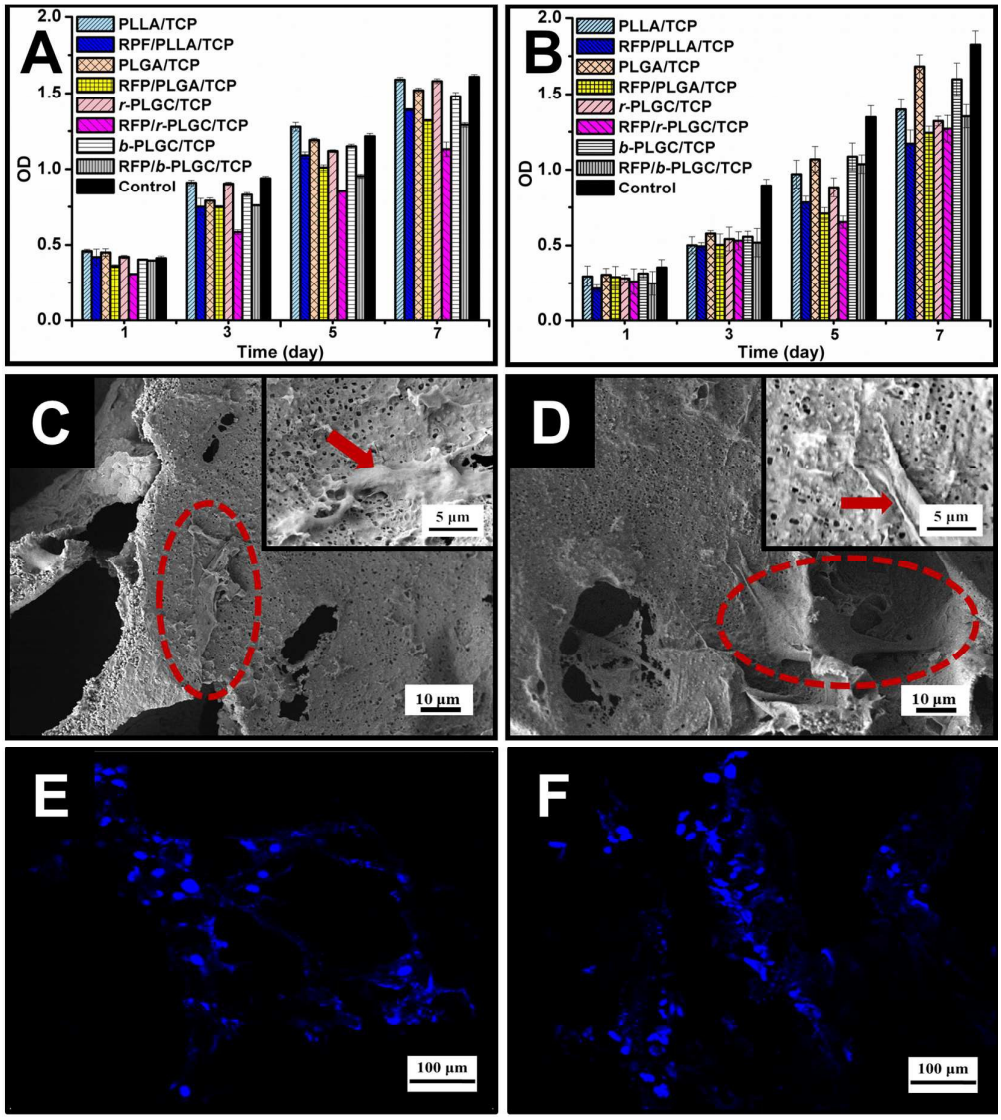

Fig. 4 Proliferation of MC3T3-E1 cells in extracting liquids of polylactone/TCP scaffolds, using DMEM as control (A); Cell proliferation of MC3T3-E1 cells on polylactone/TCP scaffolds, using tissue culture polystyrene (TCPS) as control (B); SEM images and laser confocal images showing MC3T3-E1 cell morphology on RFP/*b*-PLGC/TCP scaffold (C, E) and *b*-PLGC/TCP scaffold (D, F) after culture for 3 days.

The cell proliferation in different extracts is shown in Fig. 4(A). Without RFP loading, the aforementioned four polylactone/TCP scaffolds demonstrated comparable cell proliferation rates with insignificant difference. For all the RFP-loaded

polylactone/TCP scaffolds, cell proliferation could be seen slightly slower than those on corresponding scaffolds without RFP. Among them, the cells cultured in the extracts of RFP/*r*-PLGC/TCP scaffold demonstrated the slowest cell proliferation rate. The reason was suggested due to the fast RFP release from rubbery *r*-PLGC/TCP scaffold at 37 ^{o}C and the resulting high RFP concentration in the extract.

When MC3T3-E1 cells were co-cultured on different polylactone/TCP scaffolds, the cells could be seen proliferated continuously on all scaffolds during the 7 days culture (Fig. 4(B)). Although the cell proliferation on RFP-loading groups were inferior to those on no RFP-incorporated groups, the cell numbers on all the scaffolds had been almost three times on day 7 in comparison with those on day 1. The data indicated that the cells were viable on all the scaffolds and RFP only had limited adverse effect on the growth of MC3T3-E1 cells. After 3 days culture, the morphology of cells co-cultured on *b*-PLGC/TCP and RFP/*b*-PLGC/TCP scaffolds were observed by SEM (Fig. 4(C,D)), and the distribution of cells were observed by CLSM (Fig. 4(E,F)). Cells could be seen attaching firmly and spreading well on the scaffolds, and there were little difference in cell morphology between the two cases. The results revealed that RFP/polylactone/TCP scaffolds possessed acceptable cell affinity, showing no obvious inhibitory effects on pre-osteoblast growth.

3.5 Bone regeneration with RFP/*b*-PLGC/TCP scaffold

RFP/*b*-PLGC/TCP scaffold had shown both good cytocompatibility and long-term sustained RFP release in *in vitro* tests, therefore, it is envisioned a promising substrate to treat bone-TB *in vivo*. The evaluation of RFP/*b*-PLGC/TCP scaffold inducing bone regeneration was conducted with a critical-sized segmental defect in the forelimb of rabbit, using *b*-PLGC/TCP scaffold as comparison and untreated defect as control.

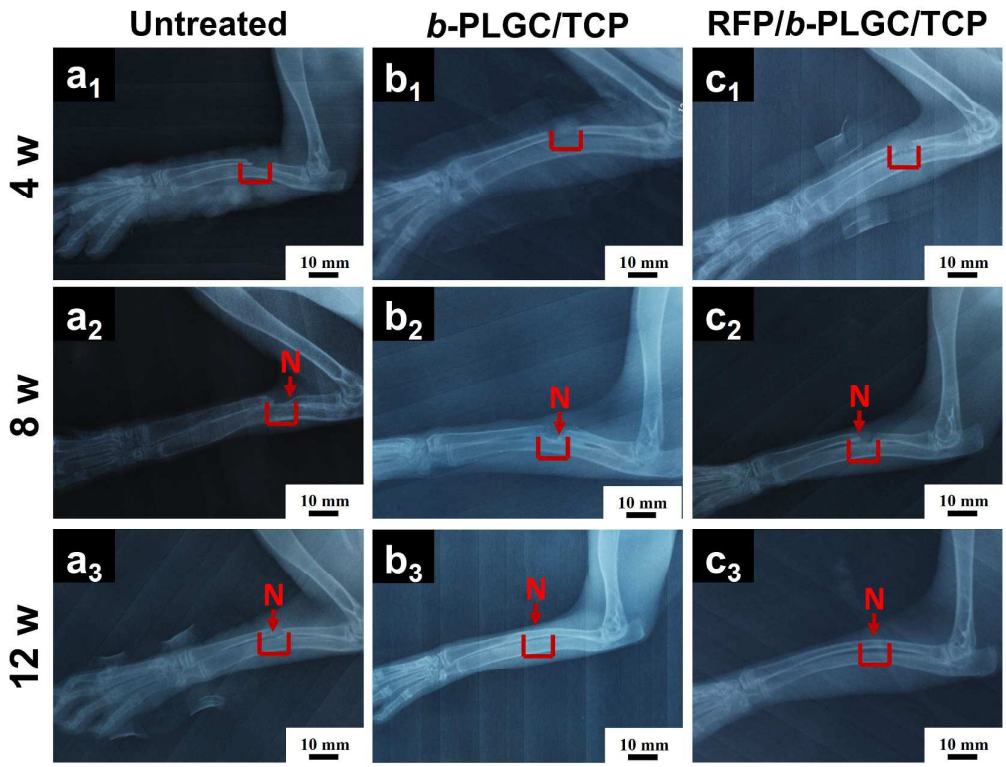

Fig. 5 Radiographs of defect sites in radius of rabbits obtained by X-ray examination after surgery for 4 weeks (a_1, b_1, c_1), 8 weeks (a_2, b_2, c_2) and 12 weeks (a_3, b_3, c_3). N: new bone.

Fig. 5 displays the radiographic images of radius bone of anesthetized rabbits in a prone position at 4, 8, 12 weeks post-operation, respectively. Radiopacity could be barely observed in the defect sites at 4 weeks for the three groups. At 8 weeks post-operation, obvious callus could be found to gradually bridge the distal ends of the defects in all cases, indicating the defects had been partially filled by new bone.[50] However, the radiopaque areas of the two scaffold-treated groups were found bigger than that of the untreated group. At 12 weeks after surgery, new bone with high degree grey-scale obviously increased in central area of defect in the two scaffold-treated groups, while there was still a blank region in the untreated group. The results demonstrated that the implantation of composite scaffolds could promote new bone growth. It suggested that the newly formed bone tissue had grown into cortical bone

in the two scaffold-treated groups, and scaffold should have degraded to give place to the newly formed bone.[51,52] No significant difference could be detected between the two scaffold-treated groups, indicating no adverse effect of releasing RFP on osteogenesis.

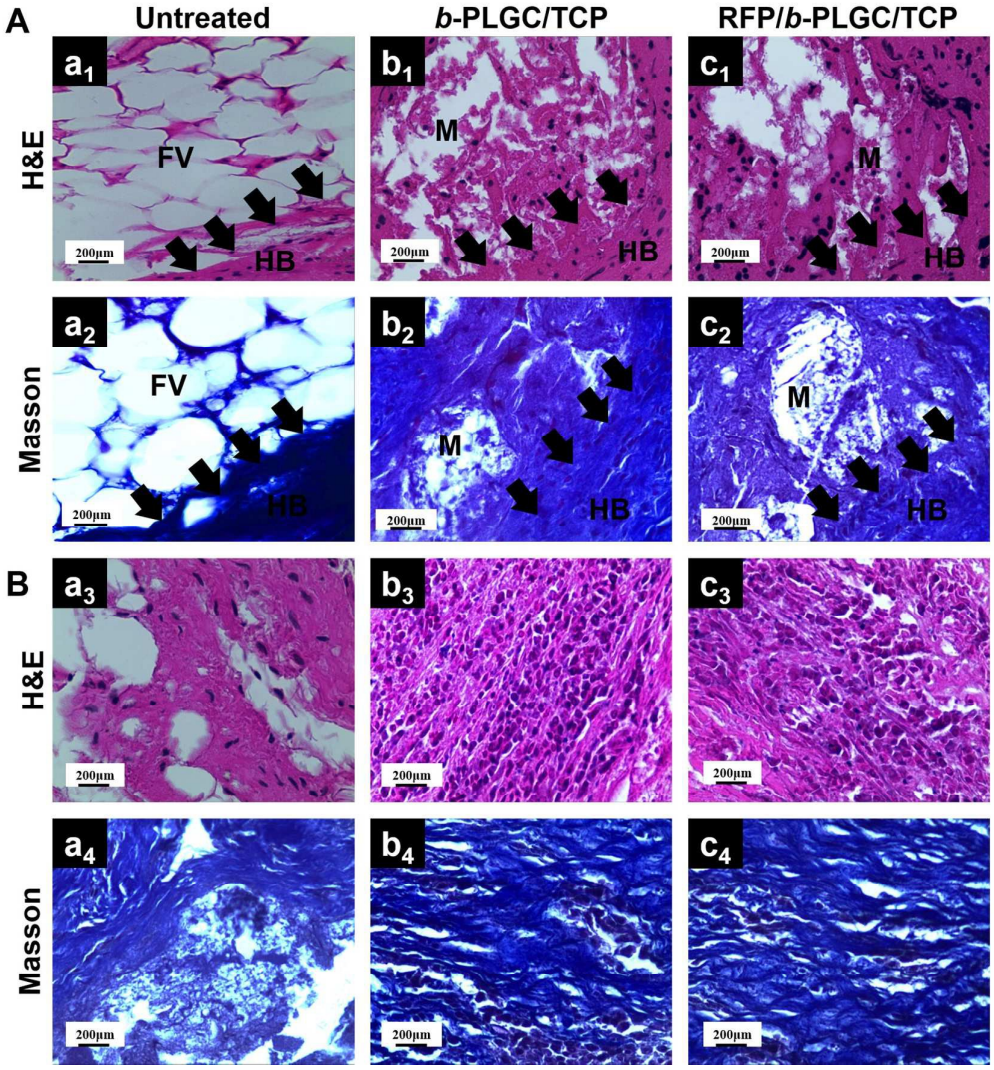

Fig. 6 Histological analysis of new formed bone sections at 4 weeks (A) and 12 weeks (B) after the surgery. (a_1, b_1, c_1, a_3, b_3, c_3) H&E staining; (a_2, b_2, c_2, a_4, b_4, c_4) Masson's trichrome staining; (a) untreated; (b) *b*-PLGC/TCP scaffold treated; (c) RFP/*b*-PLGC/TCP scaffold treated; Black arrows denote the boundary between nascent bone and host bone. (M: material; HB: host bone; FV: fat vacuoles).

Subsequently, histological assay and immunohistochemical analysis were applied to assess the newly formed bone in details. H&E and Masson's trichrome staining results were shown in Fig. 6, and the OC immunohistochemical staining results were displayed in Fig. 7. As shown in Fig. 6(A), the boundary between the defect area and the host bone tissue could still be clearly identified (marked by black arrows) at 4 weeks after surgery in all the three groups. In the untreated group, numerous fat vacuoles could be observed, showing little new osteoid tissue in the defect area. In both scaffold-treated groups, however, the defect regions had been filled with immature osteons. Substantial new bone formation was observed at the boundary of host bone bed and some cavities were formed due to the degradation of the scaffold, thus providing a benefit space for tissue in-growth and the delivery of nutrition.[53,54] In Masson staining, the formation of collagen fibers was confirmed by the blue staining in the defect area.[22] At weeks 12 post-surgery, new bone formation in the central area of the defects could be observed in three groups (Fig. 6(B)). However, the trend of new bone formation in scaffold-treated groups was more distinctive than that in the untreated group. Moreover, part of the newly formed osteoid had developed into mature cortical bone, which coalesced well with the host bone in both scaffold-treated groups. There was no obvious difference in new bone formation between the two scaffold-treated groups, which was consistent with the result of radiographic assessment. According to the Masson staining, the scaffold-treated defects were completely covered by the new bone and the blue ossein distributed uniformly in the new bone matrix.

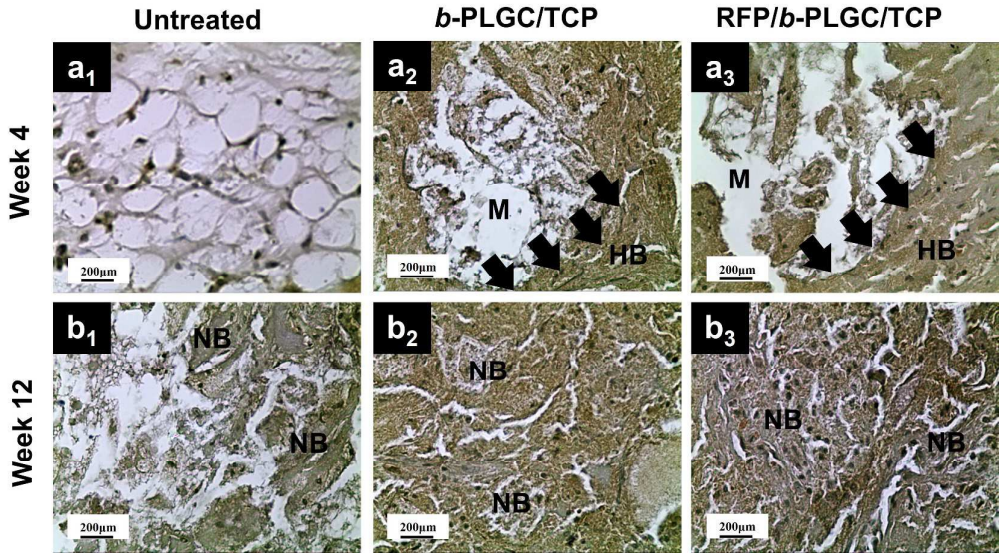

Fig. 7 Immunohistochemistry staining of osteocalcin (OC) activity on deparaffinized sections at 4 weeks (a_1, a_2, a_3) and 12 weeks (b_1, b_2, b_3) after the surgery.

OC is a kind of bone formation-related protein, appearing in the matrix of compact bone, less in cancellous bone and very rare in osteoid.[55] As shown in Fig. 7, the brown areas indicated the presence of OC in the three groups, and their differences in OC expression level could be revealed by the area of the staining. Obviously, the two scaffold-treated groups displayed stronger and larger staining than the untreated group. The defect area was further quantified using a web application software ImunoRatio, and the results were shown in Fig. 8. The OC staining intensities could be seen increasing with longer implantation time. However, at both 4 weeks and 12 weeks post-surgery, the OC staining intensity in the untreated group was much lower than those in scaffold-treated groups, which demonstrated comparable OC staining results. Summarized from all these *in vivo* evaluations, the addition of RFP in scaffold had no significant adverse effect on the osteogenesis ability of the scaffold.

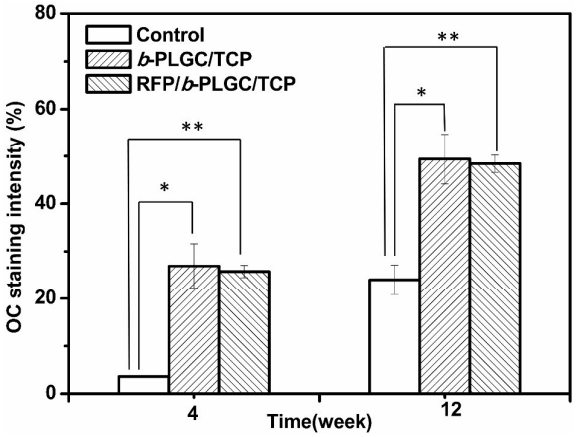

Fig. 8 Staining intensity of osteocalcin (OC) production in rabbit bone defects at 4 weeks and 12 weeks after the surgery (*P < 0.01 and **P < 0.005, comparison made between control groups and the scaffold treated group at each time-point, n = 3).

4. Conclusion

In this research, *b*-PLGC was synthesized by two steps of ring-opening polymerization. It showed many differences from corresponding *r*-PLGC copolymers in thermal behaviors, hydrophility/hydrophobicity. A composite scaffold drug delivery system was then fabricated by physical blending RFP, *β*-TCP and *b*-PLGC. The *in vitro* drug release experiment showed that hydrophobic RFP could be released from *b*-PLGC/TCP scaffold in a sustained manner for 84 days. Accordingly, RFP concentrations obtained in blood and tissue surrounding the implant could reach a high value for 12 weeks, which was above the effective level required for TB treatment. The cytological assay indicated that the RFP-loaded scaffold possessed a good cell cytocompatibility. The result of rabbit radius repair experiment displayed that composite system had good ability in bone regeneration. In conclusion, *b*-PLGC/TCP scaffold can achieve local long-term drug release and osteogenesis capability, which is potential to clinical application.

Acknowledgements

The authors acknowledge funding from the National Natural Science Foundation of China (81071454, 51473016), the National Key Technology R&D Program (2014BAI11B04), the foundation of the 309th Hospital of PLA (2013ZD-003), the Youth Foundation of the General Logistics Department (4241287K).

Note and references

[a]*Beijing Laboratory of Biomedical Materials, Beijing University of Chemical Technology, Beijing 100029, PR China*

[b]*State Key laboratory of Polymer Physics & Chemistry, Beijing National Laboratory for Molecular Sciences, Institute of Chemistry, Chinese Academy of Sciences, Beijing 100190, PR China*

[c]*Orthopaedic Department, The 309th Hospital of PLA, Beijing 100191, PR China*

[1]*These authors contributed equally to this work.*

1 D. G. Russell, C. E. Barry 3rd and J. L. Flynn, *Science,* 2010, **328,** 852-856.

2 *World Health Organization,* World Health Organization. Global tuberculosis report 2014.

3 R. K. Garg and D. S Somvanshi, *J. Spinal Cord Med.,* 2011, **34,** 440-454.

4 S. Ramachandran, I. J. Clifton, T. A. Collyns, J. P. Watson and S. B. Pearson, *Int. J. Tuberc. Lung Dis.,* 2005, **9,** 541-544.

5 M. Steyn, Y. Scholtz, D. Botha and S. Pretorius, *Tuberculosis,* 2013, **93,** 467-474.

6 P. R. Donald, *J. Infection,* 2011, **62,** 411-439.

7 M. He, H. Xu, J. Zhao and Z. Wang, *Spine J.,* 2014, **14,** 619-627.

8 M. Zhu, H. X. Wang, J. Y. Liu, H. L. He, X. G. Hua, Q. J. He, L. X. Zhang, X. J. Ye and J. L. Shi, *Biomaterials,* 2011, **32,** 1986-1695.

9 B. Saifullah, M. Z. Hussein and S. H Al Ali Hussein, *Int. J. Nanomed.,* 2012, **7,** 5451-5463.

10 T. Schaberg, *Eur. Respir. J.,* 1995, **9,** 1247-1249.

11 I. Suarez-Garcıa and A. Noguerado, *Int. J. Infect. Dis.,* 2012, **16,** 774-778.

12 I. P. Kaur and H. Singh, *J. Control Release,* 2014, **184,** 36-50.

13 A. M. Ginsberg, *Tuberculosis,* 2010, **90,** 162-167.

14 P. A. Aristoff, G. A. Garcia, P. D. Kirchhoff and H. D. Hollis Showalter, *Tuberculosis,* 2010, **90,** 94-118.

15 J. R. Weiser and W. M. Saltzman, *J. Control Release,* 2014, **190,** 664-673.

16 A. Santos, M. S. Aw, M. Bariana, T. Kumeria, Y. Wang and D. Losic, *J. Mater. Chem. B,* 2014, **2,** 6157-6182.

17 L. Kyllönen, M. D'Este, M. Alini and D. Eglin, *Acta Biomater.,* 2015, **11,** 412-434.

18 R. Cancedda, P. Giannoni and M. Mastrogiacomo, *Biomaterials,* 2007, **28,** 4040-4050.

19 G. S. Lee, J. H. Park, U. S. Shin and H. W. Kim, *Acta Biomater.,* 2011, **7,** 3178-3186.

20 P. Y. Zhou, X. S. Cheng, Y. Xia, P. F. Wang, K. D. Zou, S. G. Xu and J. Z. Du, *ACS Appl. Mater. Interfaces,* 2014, **6,** 20895-20903.

21 C. K. Williams, *Chem. Soc. Rev.,* 2007, **36,** 1573-1580.

22 H. Shen, Y. G. Niu, X. X. Hu, F. Yang, S. G. Wang and D. C. Wu, *J. Mater. Chem. B,* DOI: 10.1039/c5tb00167.

23 J. H. Shim, S. E. Kim, J. Y. Park, J. Kundu, S. W. Kim, S. S. Kang and D. W. Cho,

Tissue Eng. Part A, 2014, **20,** 1980-1992.

24 J. H. Shim, M. C. Yoon, C. M. Jeong, J. Jang, S. I. Jeong, D. W. Cho and J. B. Huh, *Biomed. Mater.,* 2014, **9**, 65006-65014.

25 G. D. Song, P. Habibovic, C. Y. Bao, J. Hu, C. A. van Blitterswijk, H. P. Yuan, W. Y. Chen, H. H. Xu, *Biomaterials,* 2013, **34,** 2167-2176.

26 M. Lin, L. Zhang, J. C. Wang, X. Y. Chen, X. Y. Yang, W. G. Cui, W. Zhang, G. J. Yang, M. Liu, Y. Zhao, C. Y. Gao and Z. R Gou, *J. Mater. Chem. B,* 2014, **2,** 2030-2038.

27 S. Samavedi, A. R. Whittington and A. S. Goldstein, *Acta Biomater.,* 2013, **9,** 8037-8045.

28 C. Erisken, D. M. Kalyon and H. Wang, *Biomaterials,* 2008, **29,** 4065-4073.

29 K. Du and Z. H. Gan, *J. Mater. Chem. B,* 2014, **2,** 3340-3348.

30 Y. Hu, X. Y. Gu, Y. Yang, J. Huang, M. Hu, W. K. Chen, Z. Tong and C. Y. Wang, *ACS Appl. Mater. Interfaces,* 2014, **6,** 17166-17175.

31 M. R. Jung, I. K. Shim, H. J. Chung, H. R. Lee, Y. J. Park, M. C. Lee, Y. I. Yang, S. H. Do and S. J. Lee, *J. Control Release,* 2012, **162,** 485-491.

32 A. Petit, M. Sandker, B. Müller, R. Meyboom, P. van Midwoud, P. Bruin, E. M. Redout, M. Versluijs-Helder, C. van der Lest, S. J. Buwalda,; L. Leede, T. Vermonden, R. Jan Kok,; H. Weinans and W. E. Hennink, *Biomaterials,* 2014, **35,** 7919-7928.

33 M. L. Kang, J. Ko, J. E. Kim and G. Im, *Biomaterials,* 2014, **35,** 9984-9994.

34 X. Feng, F. Lv, L. Liu, H. Tang, C. Xing, Q. Yang and S. Wang, *ACS Appl. Mater. Interfaces,* 2010, **2,** 2429-2435.

35 D. Huang, D. W. Li, T. T. Wang, H. Shen, P. Zhao, B. X. Liu, Y. Z. You, Y. Z. Ma, F. Yang, D. C. Wu and S. G. Wang, *Biomaterials*, 2015, **52,** 417-425.

36 Q. Cai, J. Z. Bei and S. G. Wang, *Polym. Adv. Technol.,* 2000, **11,** 159-166.

37 L. Zheng, F. Yang, H. Shen, X. X. Hu, C. Mochizuki, M. Sato, S. G. Wang and Y. Zhang, *Biomaterials,* 2011, **32,** 7053-7059.

38 F. Yang, W. J. Cui, Z. Xiong, L. Liu, J. Z. Bei and S. G. Wang, *Polym. Degrad. Stab.,* 2006, **91,** 3065-3073.

39 C. Vaquette, S. Ivanovski, S. M. Hamlet and D. W. Hutmacher, *Biomaterials,* 2013, **34,** 5538-5551.

40 C. Wischke, Y. Zhang, S. Mittal and S. P. Schwendeman, *Pharm. Res.,* 2010, **27,** 2063-74.

41 R. Vivek, R. Thangam, V. NipunBabu, C. Rejeeth, S. Sivasubramanian, P. Gunasekaran, K. Muthuchelian and S. Kannan, *ACS Appl. Mater. Interfaces,* 2014, **6,** 6469-6480.

42 Q. Cai, J. Z. Bei and S. G. Wang, *Polym. Adv. Technol.,* 2002, **13,** 105-111.

43 J. Odent, J. M. Raquez, E. Duquesne and P. Dubois, *Eur. Polym. J.,* 2012, **48,** 331-340.

44 T. K. Dash and V. B. Konkimalla, *J. Control Release,* 2012, **158,** 15-33.

45 D. W. Hutmacher, *Biomaterials,* 2000, **21,** 2529-2543.

46 V. Mourino and A. R. Boccaccini, *J. R. Soc. Interface,* 2010, **7,** 209-227.

47 T. V. Duncan and K. Pillai, *ACS Appl. Mater. Interfaces,* 2015, **7,** 2-19.

48 S. H. Chen, M. Lei, X. H. Xie, L. Z. Zheng, D. Yao, X. L. Wang, W. Li, Z. Zhao, A. Kong, D. M. Xiao, D. P. Wang, X. H. Pan, Y. X. Wang and L. Qin, *Acta Biomater.,* 2013, **9,** 6711-6722.

49 K. Hirota, T. Hasegawa, T. Nakajima, H. Inagawa, C. Kohchi, G. I. Soma, K. Makino and H. Terada, *J. Control Release,* 2010, **142,** 339-46.

50 N. Xu, X. Ye, D. Wei, J. Zhong, Y. Chen, G. Xu and D. He, *ACS Appl. Mater. Interfaces,* 2014, **6,** 14952-14963.

51 S. E. Gilchrist, D. Lange, K. Letchford, H. Bach, L. Fazli and H. M. Burt, *J. Control Release,* 2013, **170,** 64-73.

52 N. Harada, Y. Watanabe, K. Sato, S. Abe, K. Yamanaka, Y. Sakai, T. Kaneko and T. Matsushita, *Biomaterials,* 2014, **35,** 7800-7810.

53 J. J. Li, D. L. Kaplan and H. Zreiqat, *J. Mater. Chem. B,* 2014, **2,** 7272-7306.

54 H. Shen, H. B. Han, J. J. Hu, X. J. Zhang, J. J. Wang, W. J. Wang, C. H. Nie and H. M. Xu, *J. Mater Chem. B,* 2014, **2,** 800-813.

55 A. Bondarenko, N. Angrisani, A. Meyer-Lindenberg, J. M. Seitz, H. Waizy and J. Reifenrath, *J. Biomed. Mater. Res. Part A,* 2014, **102A,** 1449-1457.

Table of Contents